



The role of surface chemistry in determining *in vivo* biodistribution and toxicity of CdSe/ZnS core–shell quantum dots

Yuan Tang ^{a,b,c}, Songling Han ^a, Hongmei Liu ^a, Xin Chen ^{a,b,c}, Li Huang ^{a,b,c}, Xiaohui Li ^{a,b,c,*}, Jianxiang Zhang ^{a,b,c,*}

^a Department of Pharmaceutics, College of Pharmacy, Third Military Medical University, Chongqing 400038, China

^b Institute of Materia Medica, Third Military Medical University, Chongqing 400038, China

^c Center for Translational Medicine of TMMU, Third Military Medical University, Chongqing 400038, China

ARTICLE INFO

Article history:

Received 8 July 2013

Accepted 25 July 2013

Available online 9 August 2013

Keywords:

Quantum dot

Surface chemistry

Toxicity

Imaging

Drug delivery

Nanomedicine

ABSTRACT

To examine the effect of surface chemistry and surface charge on *in vivo* biodistribution and toxicity of CdSe/ZnS core–shell quantum dots (QDs), QDs with positive, negative, or PEG coating are used in this study for *in vivo* evaluation in a mouse model. The results suggest that QDs coated with cationic poly-diallyldimethylammonium chloride (PDDA) preferentially deposit in the lung other than in the liver, while the negative and PEGylated QDs render abundant accumulation in the liver. At higher doses positive QDs with PDDA coating show severe acute toxicity due to pulmonary embolism. Independent of their surface coatings, all QDs cause injuries in specific tissues like liver, spleen, lung, and kidney, after acute and long-term exposure, and the degree of injuries is dominated by their surface properties. For the positively charged QDs, the acute phase toxicity is primarily contributed by the coating material PDDA, while coating on QDs may amplify both *in vitro* and *in vivo* toxicity of PDDA. PEGylated QDs display the slightest chronic injuries in the long-term toxicity examination in comparison to positive or negative ones.

© 2013 Elsevier Ltd. All rights reserved.

1. Introduction

Inorganic nanoparticles have attracted increasing interest for biomedical applications, such as serving as noninvasive agents for medical imaging and as therapeutic tools for drug/gene delivery, labeling cells for cellular tracking, and biosensing changes of intracellular biological signals [1]. Besides their advantages of easy production and purification, controlled shape and size, and excellent storage stability, these nanostructured materials have showed their special capability to break through certain cellular and tissue barriers, including the cell wall in plant cells, the skin, the intestinal epithelium, the blood–brain barrier, and the placenta tissue among others [2–5]. For biomedical and pharmaceutical applications, toxicity is a critical issue to be considered when we evaluate the potentials of various nanoparticles [6]. Much attention has been therefore focused on the toxicological examination of a large

number of nanoparticles with various physicochemical characteristics. For example, the influence of size, shape, surface charge, surface chemistry, and surface topography of nanoparticles as well as experimental conditions like cell lines used and analysis methods employed have been investigated based on diverse nanoparticles and various cell lines [7–11]. To date, many findings have been obtained by cell-culture experiments [12–14]. In the case of *in vivo* toxicological studies, most of them have focused on the effects of nanoparticles that enter the body accidentally, such as by unintended exposure to airborne nanosized particles [15–17]. Only limited studies have been performed to explore the adverse effects of nanoparticles that are deliberately administered for drug delivery or imaging. Currently, the safety and potential hazards of inorganic nanoparticles in biomedical applications remain a largely unresolved issue [6,14,15,17].

Quantum dots (QDs) are well known semiconductor nanocrystals that have been extensively investigated as visible drug carriers or imaging agents due to their unique optical properties [18–20]. Nevertheless, potential toxicity is still one of the major issues that limit the advances of QDs into clinical studies. So far, the majority of nanotoxicity studies on QDs have been concentrated on *in vitro* experiments based on cell culture systems to address their cellular uptake, intracellular trafficking, subcellular distribution, and

* Corresponding authors. Department of Pharmaceutics, College of Pharmacy, Third Military Medical University, 30 Gaotanyan Main St., Chongqing 400038, China.

E-mail addresses: lpsh008@aliyun.com (X. Li), jxzhang1980@gmail.com, jxzhang@tmmu.edu.cn (J. Zhang).

cytotoxicity as well as other biological effects upon QDs exposure [21–24]. These events have been found seriously dependent on the multiplex chemical and physical factors, including composition [7], surface chemistry [25–27], surface charge [25,26], particle size [25], and UV exposure among others [28]. Whereas *in vitro* evaluations can provide profound insights into cytotoxicity at molecular and sub-cellular levels, which are particularly valuable for *in vitro* applications of QDs and other nanoparticles, one should bear in mind that frequently *in vitro* results for one cell line can not be presumably extrapolated to the same one *in vivo*. The simplified conditions in the former case distinctly differ from that encounter in the latter case with respect to cell populations and their three-dimensional organization [29,30]. Unfortunately, only a handful of studies showed the *in vivo* biological and toxicological effects of QDs [31–38], although relatively intensive investigations have examined the transport, biodistribution, sequestration, metabolism, and clearance of QDs with various biophysicochemical properties [38–43]. The particular scarcity of studies on *in vivo* QDs toxicity strongly indicates further toxicological evaluation is urgently needed to offer comprehensive understanding on the kinetics, tissue biodistribution, and toxicology of QDs as well as their relationship with the biophysicochemical characteristics, which is crucial before the translation from laboratory innovation to clinical use can be achieved [17,44].

Currently, only limited amount of research has examined surface chemistry of QDs on their *in vivo* toxicity. In addition, few studies have been performed to interrogate their long-term effects. Accordingly, critical safety issues regarding *in vivo* applications of QDs remain to be fully addressed. We hypothesize that surface chemistry of QDs displays pivotal roles in dominating their biodistribution and acute/long-term toxicity. Herein by using CdSe/ZnS core–shell QDs with different polymer coatings we evaluated the effects of surface charge and chemistry on tissue biodistribution and acute/long-term toxicity in a mouse model.

2. Experimental section

2.1. Materials

CdSe/ZnS quantum dots (QDs) with positive coating (QSQ620), negative coating (QSH620), and polyethylene glycol (PEG) coating (QMG620) were purchased from Ocean NanoTech, LLC (USA). The same batch of low molecular weight (Mw) polydiallyldimethylammonium chloride (PDDA) that was used to prepare QSQ620 (from Sigma) was kindly supplied by Ocean Nanotech, LLC (USA). Bovine serum albumin (BSA) was purchased from Sigma. 4', 6-Diamidino-2-phenylindole (DAPI) was purchased from Invitrogen (USA).

2.2. Fabrication of CdSe/ZnS QDs with various surface coatings

Firstly, CdSe core nanocrystals with emission wavelength at 620 nm were synthesized according to the well-established method [45,46]. To this end, the mixture of appropriate amount of CdO, stearic acid, and 1-octadecene (ODE) was heated to 250 °C to give a colorless clear solution. After the solution was cooled to room temperature, octadecylamine (ODA) and trioctylphosphine oxide (TOPO) were added. The obtained mixture was reheated to 280 °C under argon flow, into which a Se solution in triethylphosphine was quickly injected. The growth was carried out at 250 °C for 5 min, and then the reaction mixture was cooled to room temperature. The nanocrystals were purified by extraction to remove side products and unreacted precursors.

The successive ion layer adsorption and reaction method was followed to prepare CdSe/ZnS core–shell QDs [46]. Briefly, CdSe nanocrystals were mixed with appropriate amount of ODE and ODA, and the obtained mixture was heated to 240 °C in argon

atmosphere. Then, Zn and S precursors were separately injected to the mixture for the shell layer growth in the order of Zn–S at the 10-min interval for each injection. After the reaction mixture was cooled to room temperature, it was precipitated from acetone and extracted using hexane. Further purification of nanocrystals was performed by precipitating from acetone.

Various polymer coatings were attached to CdSe/ZnS core–shell QDs by amphiphilic polymer interdigitation approach [47]. Firstly, a triblock copolymer containing a polybutylacrylate segment, a polyethylacrylate segment, and a poly(methacrylic acid) segment (purchased from Sigma, Mw = ~100 kDa) was derivatized with octylamine (OA) to substitute about 25% of free carboxylic acid groups, by reaction in dimethylformamide using 1-ethyl-3-(3-dimethylaminopropyl) carbodiimide as the carboxyl activating reagent. ODA capped QDs were encapsulated by the amphiphilic triblock copolymer in a solvent mixture of chloroform/ethanol, taking advantage of strong hydrophobic interactions between ODA and OA. After vacuum drying, the coated dots were resuspended in an aqueous buffer and purified by gel filtration to offer QSH620. At least 120 carboxyl groups are on each QSH620 QD. QSQ620 QDs were obtained by further coating QSH620 with PDDA. On the other hand, by covalently conjugating amino-PEG (Mw = 2 kDa) with free carboxylic acid groups on QSH620 QDs, QMG620 QDs were synthesized. For both QSQ620 and QMG620, the final QDs were purified by column filtration combined with centrifugation at 6,000 g.

2.3. Characterization of CdSe/ZnS QDs

Dynamic light scattering (DLS) measurement of QDs in aqueous solution was performed with a Malvern Zetasizer Nano ZS instrument at 25 °C. The scattering angle was kept at 90° and the wavelength was set as 633 nm during whole experiments. Transmission electron microscopy (TEM) observation was carried out on a TECNAI-10 microscope (Philips, Netherland) operating at an acceleration voltage of 80 kV. The quantum yield of various QDs in aqueous solution was measured by integrating sphere. Thermogravimetric analysis (TGA) was conducted on a Mettler-Toledo TGA/DSC1 SF/177. Log P of various QDs in *n*-octanol was determined by fluorescence measurement at pH 7.4 and pH 14.

2.4. In vitro cytotoxicity

ECV304 cells were cultured in 96-well plates at a density of 5.0×10^4 /mL in 100 μL of Dulbecco's Modification of Eagle's Medium containing 10% (v/v) fetal bovine serum, 100 U/mL of penicillin and 100 μg/mL of streptomycin. Cells were incubated at 37 °C in a humidified atmosphere of 5% CO₂ for 24 h before the addition of various QDs or PDDA. Then, cells were treated with the medium containing various samples at different doses for 24 h. The cell viability was quantified by MTT method. The half maximal inhibitory concentration (IC₅₀) values were calculated by curve fitting using Originpro 7.0.

2.5. Hemolysis test

The suspension of erythrocytes in saline at 2% was prepared using freshly harvested mouse blood. Then, 2.5 mL aliquot of the erythrocytes suspension was mixed with various concentrations of QDs. The final concentration of QDs varied from 0.02, 0.04, 0.06, 0.08, to 0.1 nmol/mL. In the positive control, deionized water was added, while normal saline solution was added in the negative group. After 1 h of incubation at 37 °C, the morphology of erythrocytes was observed by scanning electron microscopy (SEM, S-3400N II, Philips, Netherland) after gradient dehydration and fixing with glutaraldehyde. Digital photos of various samples were taken

for an intuitive comparison. The hemoglobin (HGB) concentration in the supernatant was also quantified by using the BCA protein assay kit (Thermo Scientific Pierce, USA).

In addition, the hemolysis effect of QDs was examined by conducting experiments under conditions that partly mimic the microenvironment of blood vessels. To this end, an ECV304 monolayer was formed by cell culture on glass slides in a 6-well plate, onto which erythrocytes in saline at 2% were dispersed. After incubation at 37 °C for 1 h, the morphology of erythrocytes was observed by SEM.

2.6. Ex vivo fluorescence imaging

All the animal care and experimental protocols were performed in compliance with the Animal Management Rules of the Ministry of Health of the People's Republic of China (No. 55, 2001) and the guidelines for the Care and Use of Laboratory Animals of the Third Military Medical University (Chongqing, China).

Male BALB/c mice (16–20 g) were *i.v.* administered with various QDs. After predetermined time periods, mice were sacrificed and the main organs including heart, liver, spleen, lung, and kidney were resected for *ex vivo* fluorescence imaging. In the case of higher dose of QSQ620 that may lead to animal death post-administration, the organs were collected immediately after animal death. Images were collected on a CRI MaestroTM 2 *in vivo* imaging system. The excitation was carried out at 580 nm, while the emission wavelength was 620 nm.

2.7. Tissue distribution study by fluorescence microscopy

QSQ620, QSH620, and QMG620 QDs were *i.v.* administered to BALB/c mice at either 2.5 or 10 nmol/kg. In the QSQ620 group, organs including heart, liver, spleen, lung, and kidney were collected immediately after animal death, while those from QSH620 and QMG620 groups were harvested 24 h post-administration. Frozen sections of resected organs were then prepared. Confocal laser scanning microscopy (CLSM) images were taken on an Acphe Imager 5500 fluorescence microscope (Zeiss, Germany) after the nuclei were stained with 1% DAPI.

2.8. LD50 determination

BLAB/c mice (16–20 g) were used to determine the LD50 of QSQ620 and PDDA. At each dose, 10 animals comprised 5 male and 5 female mice were recruited. The highest dose for QSQ620 and PDDA was 10 nmol/kg and 14.4 mg/kg, respectively. The dose of both QSQ620 and PDDA was gradually decreased (0.8-fold gradient) until the doses at which all examined animals survived. The value of LD50 was calculated according to equation

$$\text{LD50} = \lg^{-1} \left[X_m - i \times \left(\sum P - 0.5 \right) \right]$$

where X_m is logarithm of the maximal dose, i is the difference between the logarithm values of two adjacent doses, and P is the mortality of each group.

2.9. Acute toxicity evaluation

Male BALB/c mice (16–20 g) were randomly assigned into 4 groups ($n = 10$), including one control group with saline injection and three experimental groups *i.v.* administered with QSQ620, QSH620, or QMG620 at 2.5 nmol/kg. For QDs-treated groups, 0.1 mL of various QDs in saline was injected, while 0.1 mL of saline was administered in the control group. In addition, higher dose of QSH620 and QMG620

were also injected at 10 nmol/kg. After administration, mice were weighed and their behaviors were observed for any signs of illness each day. After 14 days, animals were sacrificed by cervical dislocation after anesthesia. Blood samples were collected for the measurement of hematological parameters (Sysmex KX-21, Sysmex Co., Japan) and biochemical markers relevant to liver/kidney functions (Roche Cobas C501, Roche Co., Switzerland). Organs including heart, liver, spleen, lung, kidney, and thymus were harvested and weighed to calculate the organ index, which is defined as the percentage of the organ weight to the body weight. The histopathological sections of various organs were made after being fixed in 4% paraformaldehyde and stained with hematoxylin-eosin (H&E). Also, histopathological sections for TEM observation were prepared by fixing in 2.5% glutaraldehyde, gradient dehydration in acetone, and embedding in Epon 618. Ultrasections were then made and double stained with lead citrate and uranyl acetate. TEM observation was carried out on a TECNAI-10 microscope (Philips, Netherland).

To separate bone marrow karyocytes (BMKs) for counting, the right thighbone of each mouse from various groups was peeled off. After the two ends of the thighbone were removed, it was thoroughly rinsed with 3% acetic acid aqueous solution. Cells in the thighbone were collected, which were then suspended in acetic acid solution. The number of BMKs was counted by cell counting board after Wright's staining.

2.10. Long-term toxicity evaluation

After *i.v.* administration of various QDs at either 2.5 or 10 nmol/kg, the long-term toxicity test was performed based on male BALB/c mice. Four groups including the saline control, QSQ620, QSH620, and QMG620 were examined, with 6 animals in each group. After 15 weeks, all animals were sacrificed. Both blood samples and various organs were harvested for further analysis based on aforementioned procedures.

2.11. Statistical analysis

Statistical analysis was performed by SPSS15.0 using the paired, two-tailed Student's *t*-test for experiments consisting of two groups only and with one-way ANOVA with a multiple comparison method for experiments consisting of more than two groups. The $p < 0.05$ is considered to be statistical significance.

3. Results and discussion

3.1. QDs with various surface coatings

To date, few studies have examined the effect of surface chemistry and charge on the biodistribution and *in vivo* acute/long-term toxicity of QDs [38,48]. In this study, CdSe/ZnS core–shell QDs with positive, negative, and PEG coatings were employed to elucidate the influence of surface charge and chemistry on their *in vivo* distribution and toxicity profiles (Fig. 1). The same batch of CdSe/ZnS nanocrystals with emission wavelength at 620 nm was utilized to fabricate QDs with different coatings. According to TEM observation and statistical analysis, the average size of inorganic CdSe/ZnS core is about 8 nm. Calculation using the equation

$$D = (1.6122 \times 10^{-9})\lambda^{-4} - (2.6575 \times 10^{-6})\lambda^3 + (1.6242 \times 10^{-3})\lambda^2 - (0.4277)\lambda + (41.57)$$

(where D (nm) is the diameter of a given nanocrystal sample, and λ (nm) is the wavelength of the first excitonic absorption peak of the

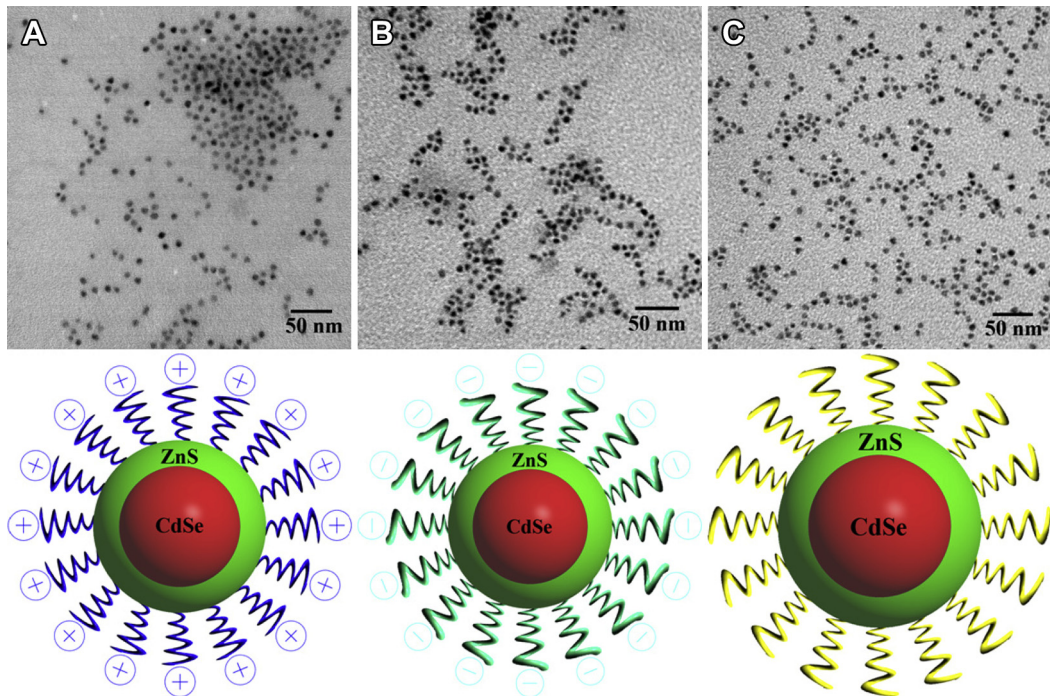


Fig. 1. CdSe/ZnS core–shell QDs with different surface coatings. A, Positively charged QSQ620. B, Negatively charged QSH620. C, PEGylated QMG620. The upper and lower panels show TEM and schematic images for the corresponding QDs, respectively.

corresponding sample), indicated that the size of 5.5 nm corresponds to fluorescence emission at 620 nm for CdSe nanocrystals [49]. Therefore, the thickness of ZnS shell was about 2.5 nm, corresponding to about 8 monolayers of ZnS, in view of the fact that the single ZnS shell thickness is about 0.31 nm. Negatively charged QDs (QSH620) were obtained through amphiphilic copolymer interdigitation approach, while further coating QSH620 QDs via a cationic polymer PDDA gave rise to QSQ620. On the other hand, PEGylated QMG620 QDs were produced by covalently conjugating 2 kDa-PEG onto carboxyl groups-coated QSH620 QDs.

The physicochemical properties of these QDs are listed in Table 1. According to measurements by DLS, the hydrodynamic diameter (D_h) was 20.0, 13.8, and 26.9 nm for QSQ620, QSH620, and QMG620, respectively. On the other hand, combination of the TEM-based core size and the thickness of organic layers showed more comparable size for three types of QDs (Table 1). This suggested that D_h was increased after surface coating with various organic moieties. The stability of QDs was examined by DLS and TEM after 6 months of storage. No significant increase in D_h could be found after this long-term storage (Fig. S1A). In addition, we did not observe obvious aggregation from TEM images (Fig. S1B–D). Consequently, QDs with these polymer coatings are highly stable in aqueous solution for at least 6 months. Whereas CdSe/ZnS nanocrystals

without hydrophilic coatings can be easily dispersed in lipophilic solvents such as chloroform and toluene, the hydrophilically coated QSQ620, QSH620, and QMG620 QDs could be scarcely dispersed in hydrophobic phases as suggested by the Log P values in *n*-octanol/water at pH 7.4 and 14 (Fig. S2). This also implied that the polymer coatings on various QDs were stable at various pH conditions.

3.2. Animal livability and tissue distribution

3.2.1. Animal livability

Firstly, animal mortality was detected using BALB/c mice after bolus injection of various QDs into the tail vein. The highest dose administered was 10 nmol/kg. This dose is equal to that used previously by others [41,50–52], which is sufficient for studying clearance kinetics, tumor targeting, and biomedical imaging post *i.v.* administration. It should be emphasized that this dose is significantly lower than that administered in some previous studies for biodistribution, imaging, and *in vivo* toxicity [32–36,39,53]. As the dosage varied from 4.096, 5.12, 6.4, 8, to 10 nmol/kg, significant difference in mortality was observed for various groups (Fig. 2A). For QSQ620-treated mice, no animal death occurred at doses below 6.4 nmol/kg, while half mice died at 6.4 and 8 nmol/kg. At 10 nmol/kg, the mortality was 100% (Fig. 2B). For mice treated with QSQ620,

Table 1

Physicochemical properties of CdSe/ZnS core–shell QDs employed in this study.

QDs	Size ^a (nm)	D_h (nm)	Surface chemistry	ζ -potential (mV)	Quantum yield ^d
QSQ620	8.1	20.0 ^b ; 22.1–24.1 ^c	=N ⁺ (CH ₃) ₂ Cl [−]	>+50	>50%
QSH620	7.9	13.8 ^b ; 15.9–17.9 ^c	−COOH	−30 to −50	>50%
QMG620	7.9	26.9 ^b ; 19.9–21.9 ^c	PEG	−10 to 0	>50%

^a Diameter based on TEM measurements.

^b D_h , hydrodynamic diameter measured by DLS.

^c Hydrodynamic size based on TEM measurement and organic thickness indicated by the manufacturer.

^d Measured using an integrating sphere.

animal death occurred within 24 h post injection. After this critical period, the involved mice survived in the whole period of experimentation. As for mice *i.v.* injected with QSH620 or QMG620, no animal death occurred at 10 nmol/kg. Also, no death was observed even when the dose was increased to 20 nmol/kg. LD50, the dose that kills half of the animals tested, was then calculated. The LD50 of QSQ620 was 7.16 nmol/kg, while it was higher than 20 nmol/kg for both QSH620 and QMG620. This result suggested that the surface coating of QDs has a profound influence on their *in vivo* toxicity. Previously, a plethora of studies showed that the surface chemistry/charge of nanoparticles may significantly influence their cellular uptake, subcellular distribution, and cytotoxicity [7,9,11,12,14,21,23,25–29,54,55]. However, the effect of these surface properties on *in vivo* toxicity has been rarely interrogated [29,35,38,48]. Whereas PDDA and its copolymers have been broadly utilized to construct or decorate micro- and nano-structures for drug delivery, gene therapy, and antibacterial applications [56–58], our results clearly demonstrated that PDDA-coated QDs showed strikingly higher *in vivo* toxicity, when compared with either carboxyl groups or PEG chains coated QDs.

3.2.2. Tissue distribution

To clarify the reason responsible for acute animal death in the QSQ620 group, *ex vivo* fluorescence imaging was performed for the major organs resected from the died mice. For mice injected with

10 nmol/kg of QSQ620, the strongest red fluorescence was observed in the lung other than in the liver (Fig. S3A). In contrast, more intensive fluorescence was identified in the liver of mice administered with QSH620 and QMG620 at the same dose of 10 nmol/kg, while only slight red fluorescence was observed in the lung of the QSQ620-treated mouse (Fig. S3B). More intuitive results could be discerned when the major organs from all groups were imaged in the same cohort. As illustrated in Fig. 3A, the lung from the QSQ620 group exhibited the strongest fluorescence among all organs examined, which was followed by livers from QSQ620 and QMG620 groups. These results clearly indicated that QSQ620 was largely present in the lung, while QSH620 and QMG620 preferred to accumulate in the liver. Further scrutiny was carried out by CLSM observation on frozen sections from resected organs. In the heart tissue, scattered red fluorescence appeared in the QSQ620 group, while the QSH620 and QMG620 group did not show any fluorescence (Fig. 3B). For all mice administered with QDs, there were uniformly distributed fluorescence dots in the liver. Nevertheless, the QSQ620 group gave the most significant fluorescence domains in the liver and spleen. Red fluorescence could also be observed in the spleen of the QSH620 and QMG620 groups. Whereas both QSH620 and QMG620 group only exhibited disseminated red domains in the lung, marked and heterogeneous red fluorescence appeared near capillaries of the lung in the QSQ620 group. The most evident red fluorescence in the lung tissue of the QSQ620

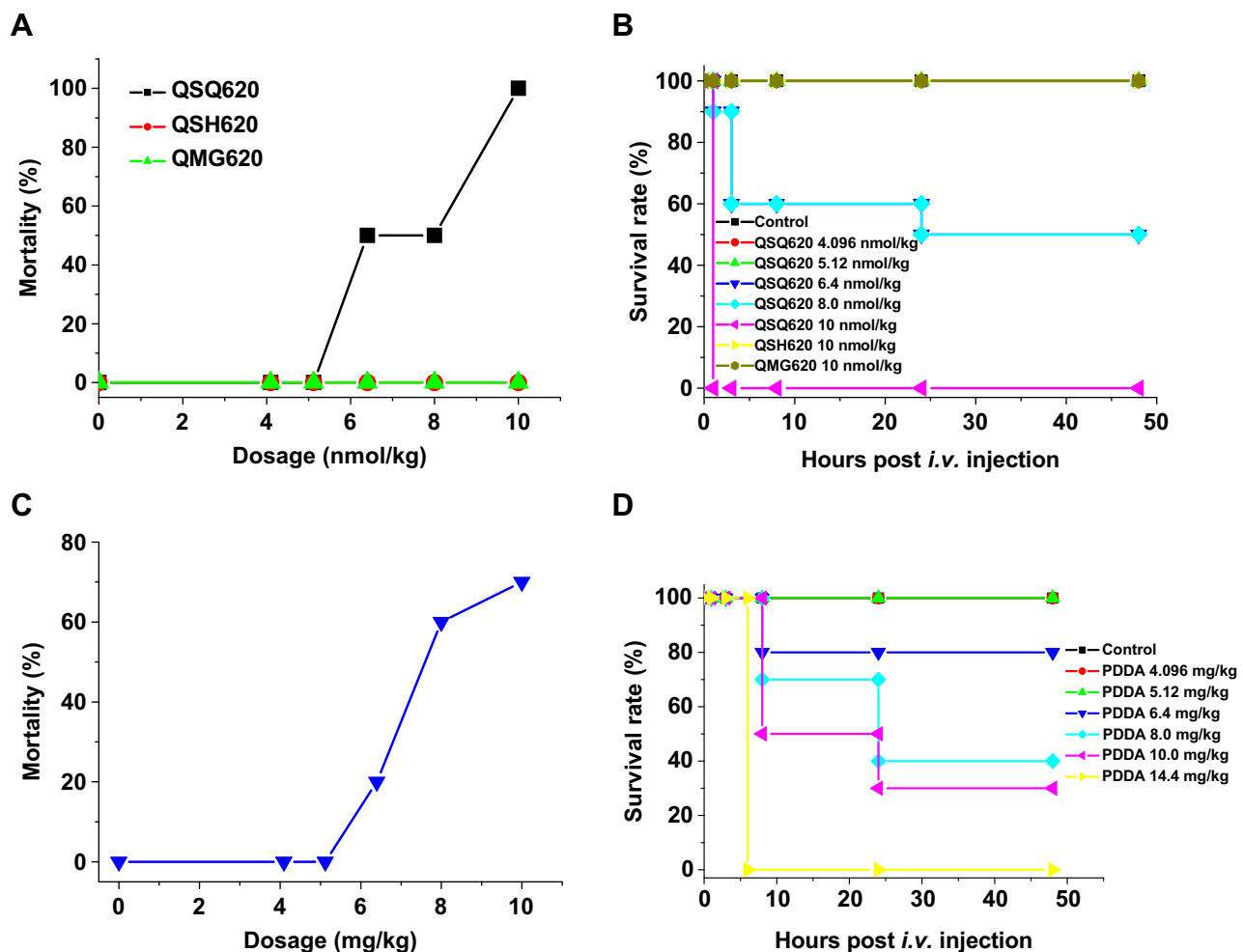


Fig. 2. Dose-dependent mortality and survival rate of BALB/c mice after *i.v.* administration of various QDs and PDDA. A–B, Dose-dependent mortality (A) and survival curves (B) in various QD groups. C–D, Mortality (C) and survival curves (D) of mice administered with various doses of PDDA.

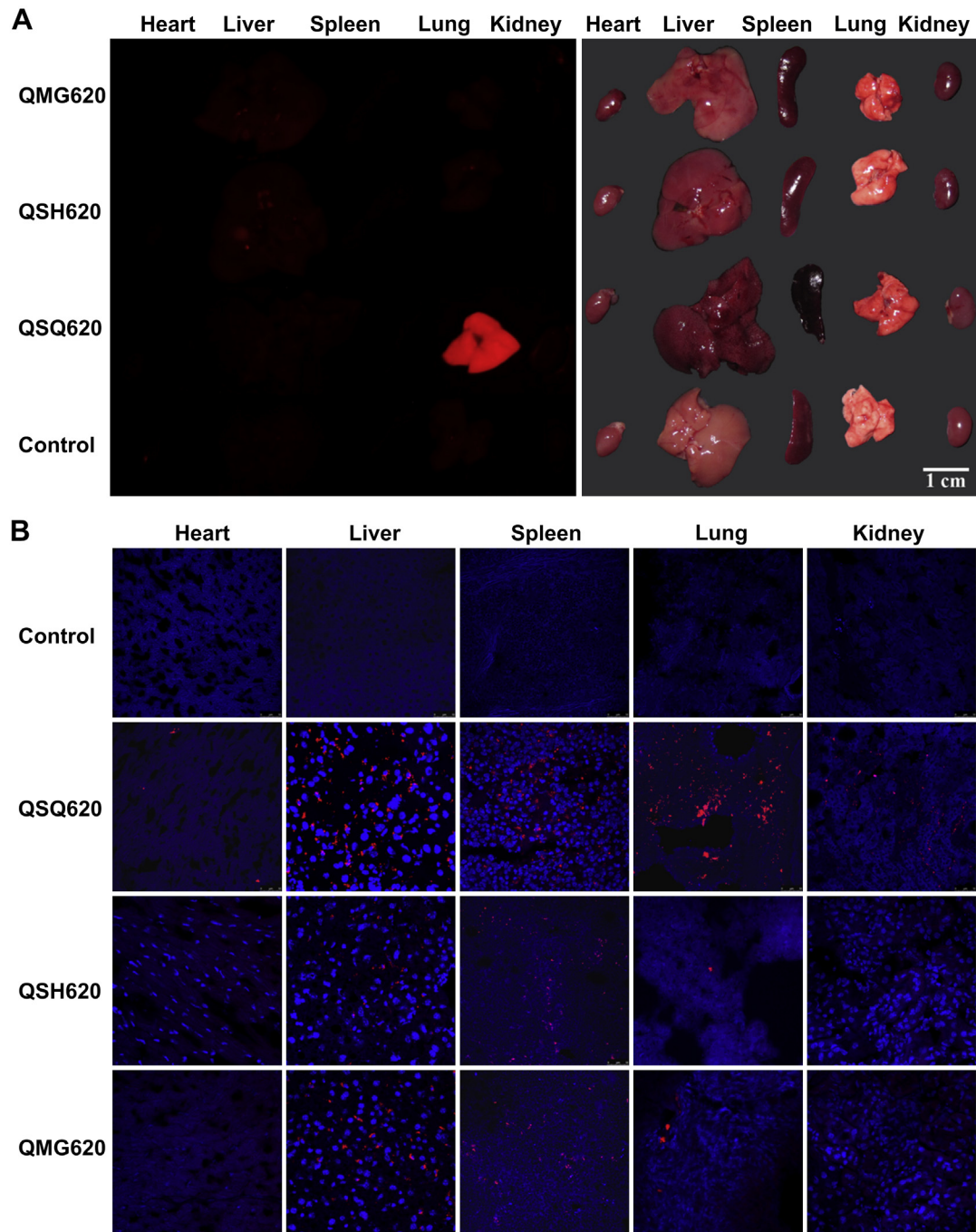


Fig. 3. QDs biodistribution study by fluorescence imaging. A, *Ex vivo* fluorescence imaging. The right panel illustrates the color video images of corresponding organs shown in the left. B, CLSM images showing frozen sections of various organs resected from mice administered with various QDs. The dose of QDs was 10 nmol/kg for all the QDs-treated groups. In the case of QSQ620 group, the organs were resected immediately after animal death, while they were collected 24 post-administration for QSH620 and QMG620 groups. The nucleus was stained with 1% DAPI for CLSM imaging.

group well agrees with the result of *ex vivo* imaging. Of note, bright fluorescence was also found in the kidney of QSQ620-treated mice. These results suggested that tissue distribution of QDs is strongly dependent on their surface chemistry. For currently involved QDs, positively charged QSQ620 would deposit in the main organs including heart, liver, spleen, lung, and kidney. On the other hand, the majority of negative and PEGylated QDs accumulated in the liver, although part of them was present in the spleen and kidney. The marked accumulation of positive QDs in the lung was unexpected, since previous studies in both mice and rats have confirmed

that negatively charged and PEGylated QDs preferentially accumulate in the liver and spleen [32,33,39–41], which is related to the clearance of nanoparticles by mononuclear phagocytic systems.

It is well known that microparticles may be directly transported to the right ventricle of the heart via the venous network after *i.v.* administration, from where they enter the pulmonary circulation [59]. The smallest blood vessels of lung capillaries constitute the first mechanical filters for the delivered particles. Accordingly, a severe pulmonary embolism may be responsible for the animal death occurred in the QSQ620 group. However, since the original D_h

of QSQ620 QDs is far below the threshold size of 2–13 μm , above which significant retention in the pulmonary capillaries may be achieved, we hypothesize that QSQ620 may form aggregates with blood components like proteins and cells, which are then physically blocked in the small capillaries of the lung.

Incubation of QSQ620 with albumin, the most abundant protein in the plasma, revealed a significant increase in the particle size (Fig. S4), while no dramatic changes were found for QSH620 and QMG620. Besides, the effect of various QDs on red blood cell (RBC) was examined, since it is the most abundant blood cell, representing 45–55% of the blood volume. A direct observation suggested that QSQ620 did not show more significant hemolysis, when compared with QSH620 and QMG620 (Fig. S5A). Quantification of HGB indicated that treatment with QSQ620 and QSH620 led to relatively higher leveled HGB release (Fig. S5B). Aggregation of RBCs occurred in the presence of QSQ620 (Fig. S5A), as indicated by relatively weak red color when the QDs concentration was increased, which was clearly in contrast to QSH620 and QMG620. This was further confirmed by microscopy observation. As illustrated in Fig. 4 and Fig. S6, significant aggregation of RBCs could be clearly observed in the case of QSQ620. This phenomenon was even more striking when RBCs with relatively low density were adopted (Fig. S7). Similar aggregation effect occurred for QSQ620-treated RBCs that were reconstituted on the monolayer of cultured ECV304 cells, which was employed to mimic the vascular endothelium (Fig. S8). Accordingly, positive QSQ620 mediated severe aggregation of plasma proteins (like albumin, lipoproteins, and complement proteins) and blood cells (RBCs, platelets, and leukocytes) as well as other blood components, which led to the formation of large thrombus, should be responsible for the capillary embolism that eventually caused acute animal death. In humans, each circulation takes about 20 s, which should be more rapid for the mouse. Owing to the rapid blood circulation, intravenously injected QDs may finish one circulation within 20 s. Therefore, the formation of

aggregates that were large enough for severe capillary occlusion should have proceeded gradually, since animal death was observed almost 1 h post injection. Of note, whereas no RBCs aggregation occurred for QSH620 and QMG620-treated groups, shrinkage of RBCs could be observed, which is similar to that resulting from hypertonic conditions. This is particularly significant as far as the QMG620 group was concerned (Fig. 4D and Fig. S7D). Consequently, when these nanoparticles are utilized *in vivo*, special attention should be paid to their deleterious effects on blood cells although they may not lead to animal death at relatively low doses.

On the other hand, the passive lung targeting reached by *i.v.* injection of nanoparticles affords another opportunity to treat pulmonary diseases from the vascular side, which is especially beneficial in situations where lung capacity is severely compromised and inhalation is not a feasible strategy [60]. Whereas our results showed that high doses of positive QDs coated with PDAA may cause severe acute toxicity by physical embolism, which may be mitigated by changing dosing regimen (for example, changing the single injection to multiple administration), lowering administered dosage, and using more biocompatible cationic materials for surface coating.

3.3. Acute toxicity

Subsequently, acute toxicity was implemented following *i.v.* injection of various QDs at 10 nmol/kg. In the case of QSQ620, all mice died within 1 h after administration. As evidenced by fluorescence imaging, animal death in this case was mainly due to dysfunction of the heart and lung, resulting from pulmonary embolism. For both QSH620 and QMG620, the experiment was performed for 14 d. Post administration, the animal body weight was monitored every two days. At each time points, no significant difference in the body weight could be found between the QDs-treated group and the control group (Fig. 5A). Observation on the

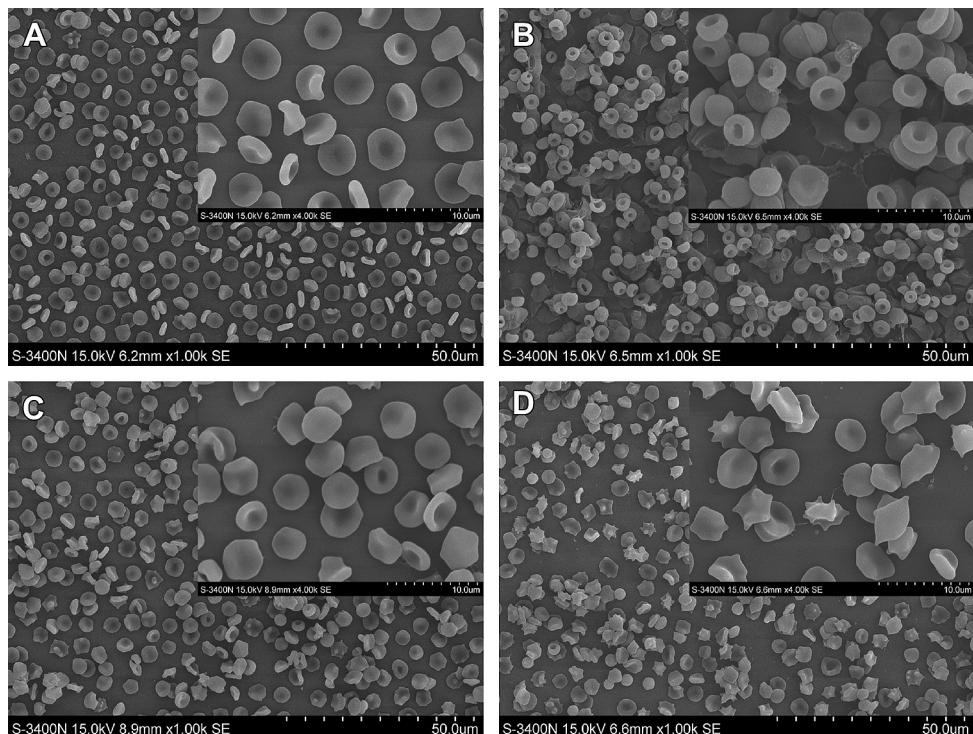


Fig. 4. SEM images of RBCs in the presence of various QDs. A, The control group that was treated with the normal saline solution; B, QSQ620; C, QSH620; and D, QMG620. The concentration of QDs was 0.1 nmol/mL. The density of RBCs was $1 \times 10^8/\text{mL}$.

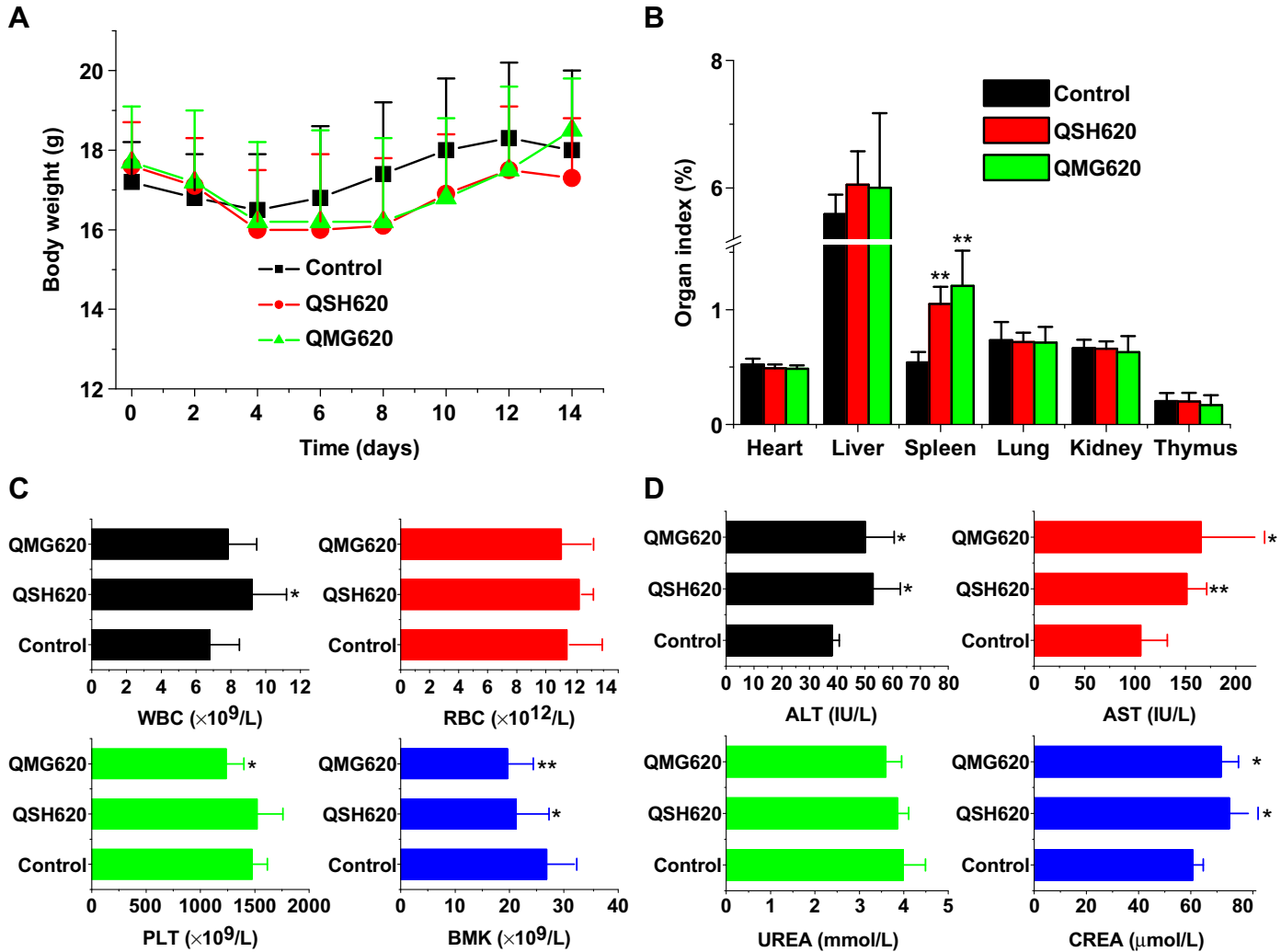


Fig. 5. Acute toxicity of QSH620 and QMG620 QDs 14 days after i.v. administration in mice at 10 nmol/kg. A, Changes in the body weight. B, The organ index. C, Hematological parameters. D, Typical biochemical parameters related to liver and kidney functions. * $p < 0.05$ versus the control group; ** $p < 0.01$ versus the control group. WBC, white blood cell; RBC, red blood cell; PLT, platelet; BMK, bone marrow karyocyte; ALT, alanine aminotransferase; AST, aspartate aminotransferase; UREA, blood urea; and CREA, creatinine. Data are mean \pm SD (SD, standard deviation; $n = 10$).

general effects suggested that the skin, hair, eyes, mucous membranes, secretion, and excreta were normal for mice in all groups. No abnormalities in eating, drinking, breath, autonomic movement and behaviors as well as responses to various stimuli were found. In addition, no symptoms of toxicosis such as somnolence, salivation, cramps, convulsions, vomiting, diarrhea, paralysis, and breathing difficulties were observed in any animals. During the test period, no animal death occurred. Two weeks post treatment, mice were sacrificed, and blood samples and major organs were harvested. The organ index of heart, liver, spleen, lung, kidney, and thymus was calculated. We found a significant increase in the spleen index for mice treated with QSH620 and QMG620 (Fig. 5B), indicating the presence of splenomegaly in these two groups. As extensively demonstrated, spleen is one of the main organs in which various nanoparticles may be accumulated [61]. Our CLSM observation also showed the splenic accumulation of QDs, as shown in Fig. 3B. Nevertheless, no significant changes in the liver index could be observed for the QDs-treated mice despite the fact that nanoparticles may also deposit in the liver, suggesting no swelling occurred in this organ.

Typical blood cells including white blood cells (WBCs), RBCs, and platelets (PLTs), as well as BMKs were counted. The number of

WBCs was increased in both QSH620 and QMG620-treated groups, whereas statistical significance was only observed in the QSH620 group (Fig. 5C). Variation in WBCs suggested that QDs-treatment may have affected the immune system or induced acute inflammatory response. No significant changes could be found for RBCs, while the number of PLTs markedly decreased in the QMG620 group. The number of BMKs was reduced for both QSH620 and QMG620-treated mice. Since all blood cells are derived from BMKs, their decrease is in agreement with decreased PLTs for the QMG620-treated group. For RBCs, they have an extremely long lifespan in circulation. In humans, normal RBCs may circulate for about 100–120 d in the body before their components are recycled by macrophages [62]. As a result, the number of RBCs did not respond to the reduced BMKs during the test period of 14 d. Quantification of selected biochemical markers showed significant increase in the levels of alanine aminotransferase (ALT) and aspartate aminotransferase (AST) in both QSH620 and QMG620 groups (Fig. 5D). Clearly, hepatocellular injury resulting from liver accumulation of QDs should account for the enhanced ALT and AST levels in circulation. The level of creatinine (CREA) was also increased markedly in QDs-treated groups. Since CREA is mainly filtered out of the blood by glomerular filtration and proximal tubular secretion, the

increased CREA level in blood reflected the decreased glomerular filtration rate, presumably resulting from injured glomerulus or proximal tubule.

Histopathological analysis of major organs was carried out based on H&E stained sections. Whereas all the mice died within a few hours post injection with QSQ620 at 10 nmol/kg, we still detected swelling hepatocytes and vesicle-like cytoplasm in some hepatocytes of the liver collected immediately after the animal death (Fig. 6A). Consistent with the immediate death after QSQ620 treatment, no discernible changes were observed for organs like heart, spleen, lung, and kidney. As for QSH620 and QMG620-

treated mice, capillary dilation and hyperaemia could be observed in the liver, while evident hyperplasia in the germinal center, augmented germinal centers, increase in the number of thickened blood vessels, as well as hyperaemia occurred in the spleen. For the lung tissue in QSH620 and QMG620 groups, capillary hyperaemia in pulmonary alveoli, enlarged alveolar space, and deflated alveolar cavity could be found (Fig. 6A). For other tissues, no significant abnormalities could be discerned. Further examination on various tissues was conducted by TEM (Fig. 6B). With the exception of swelling hepatocytes and hyperaemia in the lung, no other significant changes could be observed in sections of the

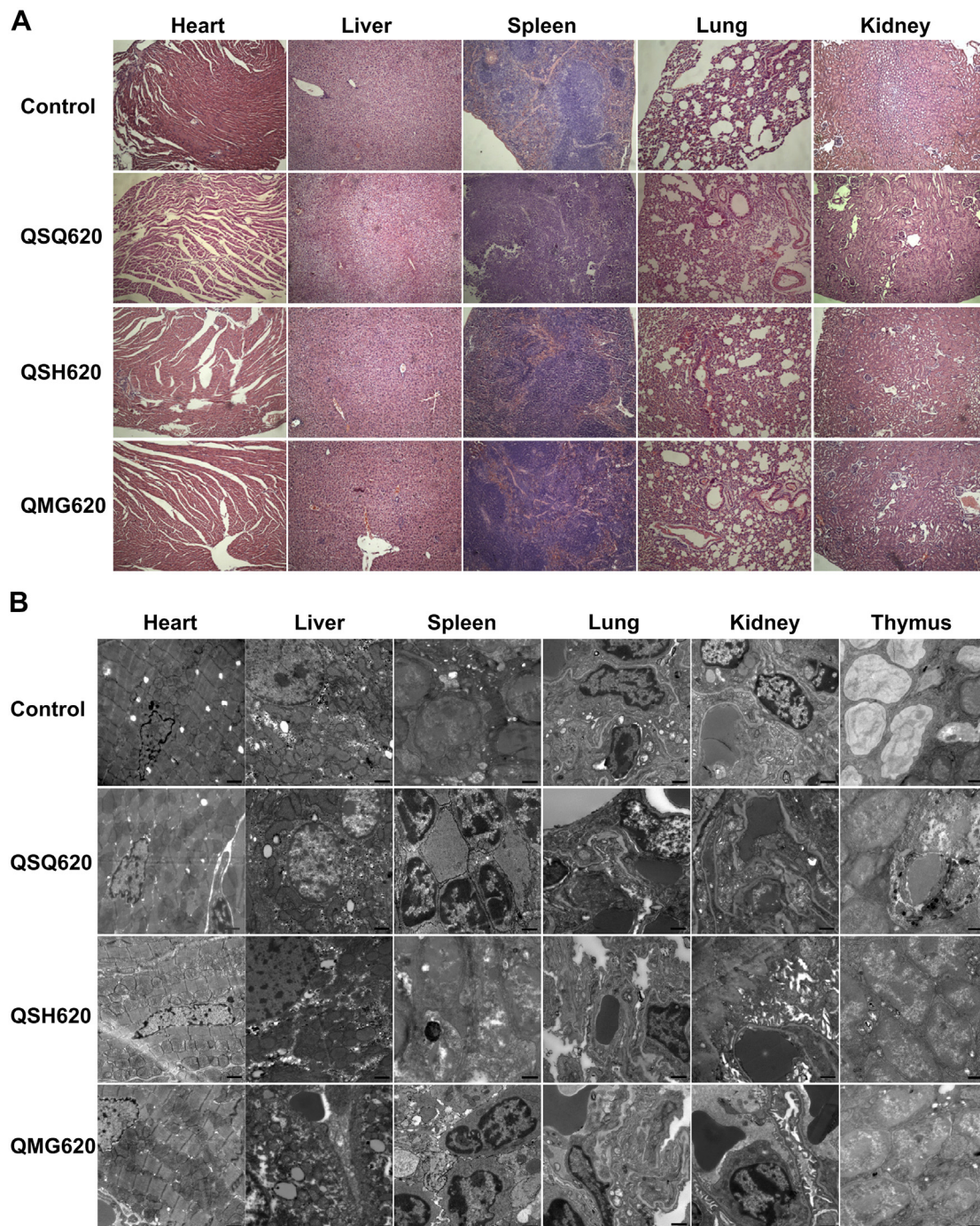


Fig. 6. Histopathological analysis of major organs resected from mice after acute toxicity evaluation at 10 nmol/kg. A, Light microscopy images of H&E sections taken at $\times 10$ magnification. B, TEM images. The scale bar represents 1 μm .

QSQ620-treated group. This agrees with results based on H&E sections. These results confirmed that animal death after QSQ620 treatment at 10 nmol/kg was due to the obstruction of blood vessels in the lung. For QSH620 and QMG620 groups, hyperaemia and hyperplasia were discerned in the spleen. In the kidney, podocytes in these two groups syncretized severely. This ultrastructure observation is in line with increased CREA level as illustrated in Fig. 5D. All injuries in the kidney might be associated with the excretion of QDs by glomerular filtration. For other tissues, no distinct abnormalities could be detected in the QSH620 and QMG620 groups.

We further compared the acute toxicity profiles of three QDs at a lower dose of 2.5 nmol/kg, at which all the QSQ620-treated mice survived. At the examined time points, we did not find significant difference in the body weight between the QDs-treated group and the control group (Fig. 7A). No abnormalities in general behaviors and no symptoms of toxicosis were observed for all the treated mice. Calculation of the organ index showed the significant increase in the spleen index of all QDs-treated mice as compared with the control group, while no dramatic difference was found for other organs

(Fig. 7B). Complete blood counting indicated that the number of WBC, RBC, and PLT as well as the HGB concentration were in the normal range in comparison to the control (Fig. 7C). As for the biochemical markers associated with liver/kidney functions, only the QSQ620 group showed significant increase in the level of CREA (Fig. 7D). Histopathological analysis on H&E stained sections were then conducted (Fig. 7E). Compared with the saline control, the liver from the QSQ620-treated mouse only showed slight inflammation and swelling of hepatocytes. Consistent with the increased spleen index, significant changes occurred in the spleen. Reactive hyperplasia, hyperaemia in the splenic sinus, and increase in the number of thickened blood vessels could be clearly identified in the QSQ620 group. As for QSH620 and QMG620, hyperplasia and hyperaemia in the splenic sinus could also be observed. No remarkable changes were detected for other organs. We also examined these tissues by TEM observation on double-stained ultrasections. As illustrated in Fig. 7F, disorganized and fragmented myofilaments were observed in the heart tissue of QSQ620-treated mice, whereas they were normal in both QSH620 and QMG620 groups. The injury of myofilaments is coincident with the presence of QDs in the heart tissue from the

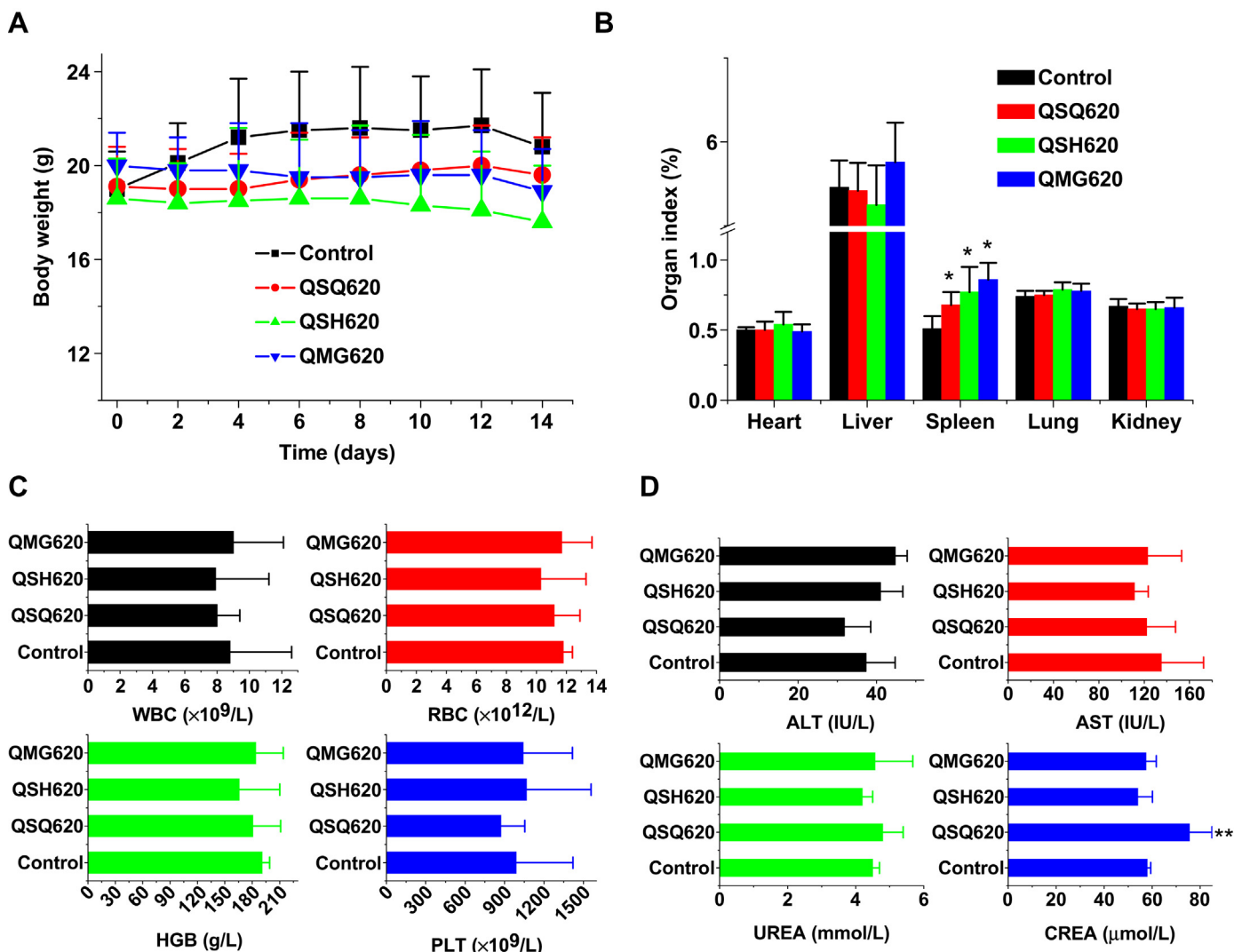


Fig. 7. Acute toxicity of various QDs after i.v. administration in mice at 2.5 nmol/kg for 14 days. A, Changes in the body weight. B, The organ index. C, Hematological parameters. D, Typical biochemical parameters relevant to liver and kidney functions. * $p < 0.01$ versus the control group; ** $p < 0.001$ versus the control group. Data are mean \pm SD ($n = 9$). E, Light microscopy of H&E sections of major organs from mice 14 days after treatment with QDs at 2.5 nmol/kg. All images were taken at $\times 10$ magnification. F, TEM images of ultrasections. The scale bar represents 1 μm .

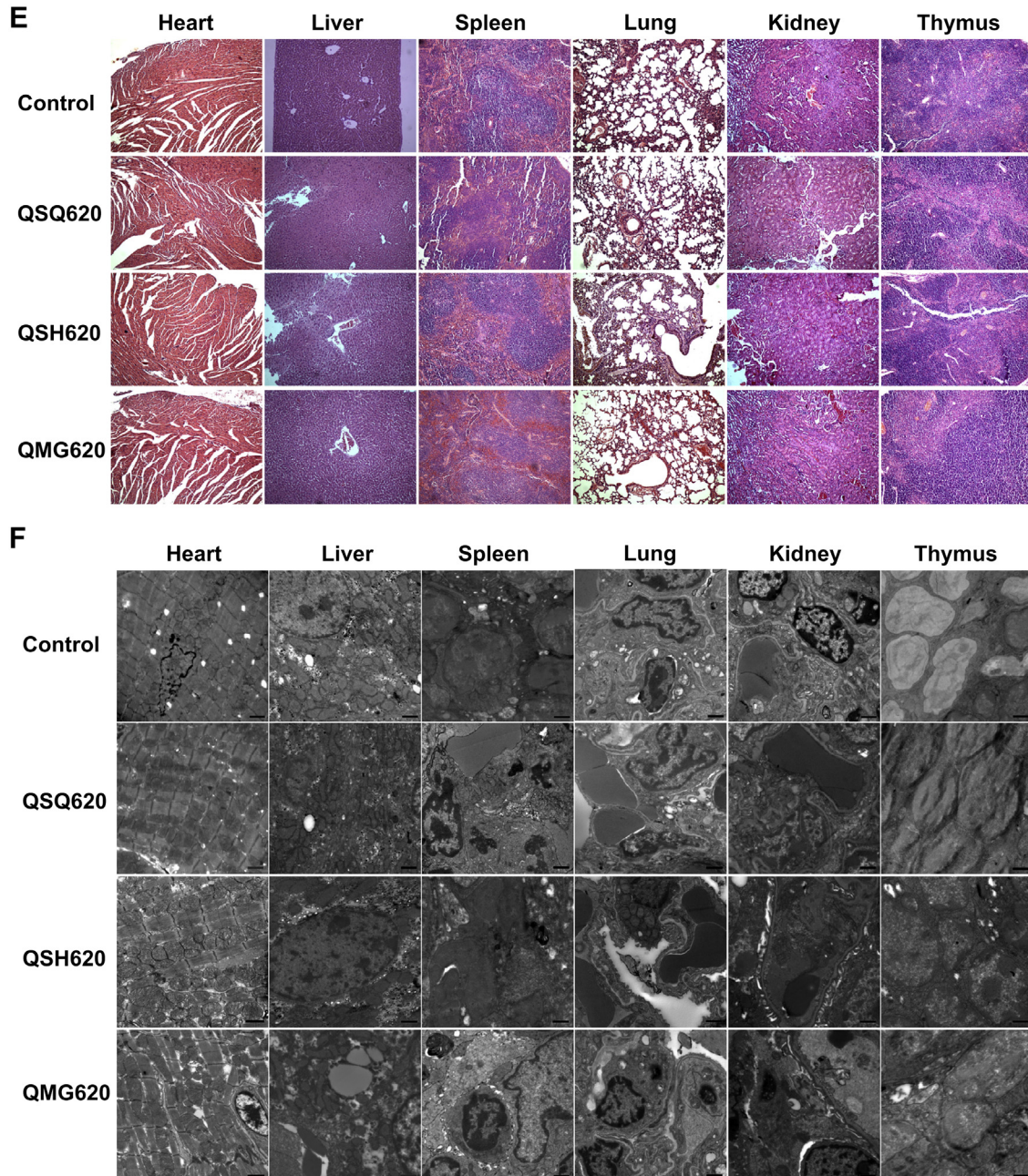


Fig. 7. (continued).

QSQ620-treated mice. Consistent with QDs distribution in the liver, the nucleus of hepatocytes became blurry for the QSQ620-treated mouse, and lysosomes increased significantly in this group. Hyperaemia and hyperplasia were discerned in the spleen of all QDs-treated groups, and the most severe effect occurred in the QSQ620 group. In addition, the nucleus of some spleen cells became debris in the QSQ620 group. As for the pulmonary tissue, evident swelling of endothelial cells was found for the QSQ620-treated mouse, while no any distinguishable abnormalities appeared in the QSH620 and QMG620 groups. In kidney, injuries were found in all QDs-administered groups. Specifically, filtration silts of podocytes disappeared completely in the QSQ620 group, while podocytes in both QSH620 and QMG620 groups syncretized. These effects are similar to

those observed at 10 nmol/kg, albeit to a slighter degree. Consistent with previous study [31], our results also indicated that investigation by electron microscopy can provide more details in comparison to observation by light microscopy. Injuries in the kidney might be associated with the excretion of QDs by glomerular filtration. For thymus tissue, no distinct abnormalities could be detected.

Taken together, this acute toxicity study indicated that *i.v.* administration of various QDs may cause injuries in different organs. Besides the dosage administered, the site and degree of injuries are seriously dependent on the surface chemistry/charge of injected QDs. The PDDA-coated positive QSQ620 showed the most severe acute toxicity at either lower or higher dose, in comparison to negative and PEGylated QDs.

3.4. Long-term toxicity

A long-term *in vivo* examination was carried out for 15 w after a single *i.v.* injection of various QDs. Initially, QSH620 and QMG620 were examined at 10 nmol/kg. The single administration of QDs did not result in evident change in the body weight 15 w post injection (Fig. S9A). Measurements on typical hematological parameters indicated decrease in the number of WBCs and RBCs after treatment with QSH620 when compared with the control (Fig. 8A). Consistent with the reduced RBCs number, the HGB level in this group was also decreased. Nevertheless, no significant variation was found for PLTs. This suggested that *i.v.* administered QDs may have affected the hemopoietic system, especially in the case of QSH620, which is partly consistent with the reduced BMKs as indicated in acute toxicity study. The QSH620 group displayed higher level of AST when compared with the control group (Fig. 8B), reflecting the existence of hepatocellular injury. On the other hand, the typical biomarkers of kidney function, i.e. UREA and CREA, showed no significant difference between the QDs-

treated group and the control group. These results suggested that the liver injuries in the QSH620 group still existed 15 w after administration.

H&E stained pathological sections of main organs including heart, liver, spleen, lung, and kidney were then made to confirm above mentioned results (Fig. 8C). In the QSH620 group, the borderline of hepatic sinuses was blurred, and straitness occurred around them. In this group, we could also observe splenic hyperfunction, reactive hyperplasia in the lymphoid follicle, and hyperaemia in the splenic sinus in the spleen. As for the QMG620-treated mouse, slight cellular edema appeared in the liver, while hyperaemia in the splenic sinus was discerned in the spleen. No evident vacuole-like pathological changes in hepatocytes were found in QSH620 and QMG620 groups. Slight thickening of the pulmonary alveolar wall and reactive hyperplasia of lymph nodes were observed in the lung of these two groups. In the kidney, hyperplasia and swelling of glomerular capillary endothelium appeared in the QDs-treated groups. Also, no distinguishable injuries occurred in other organs of these two groups.

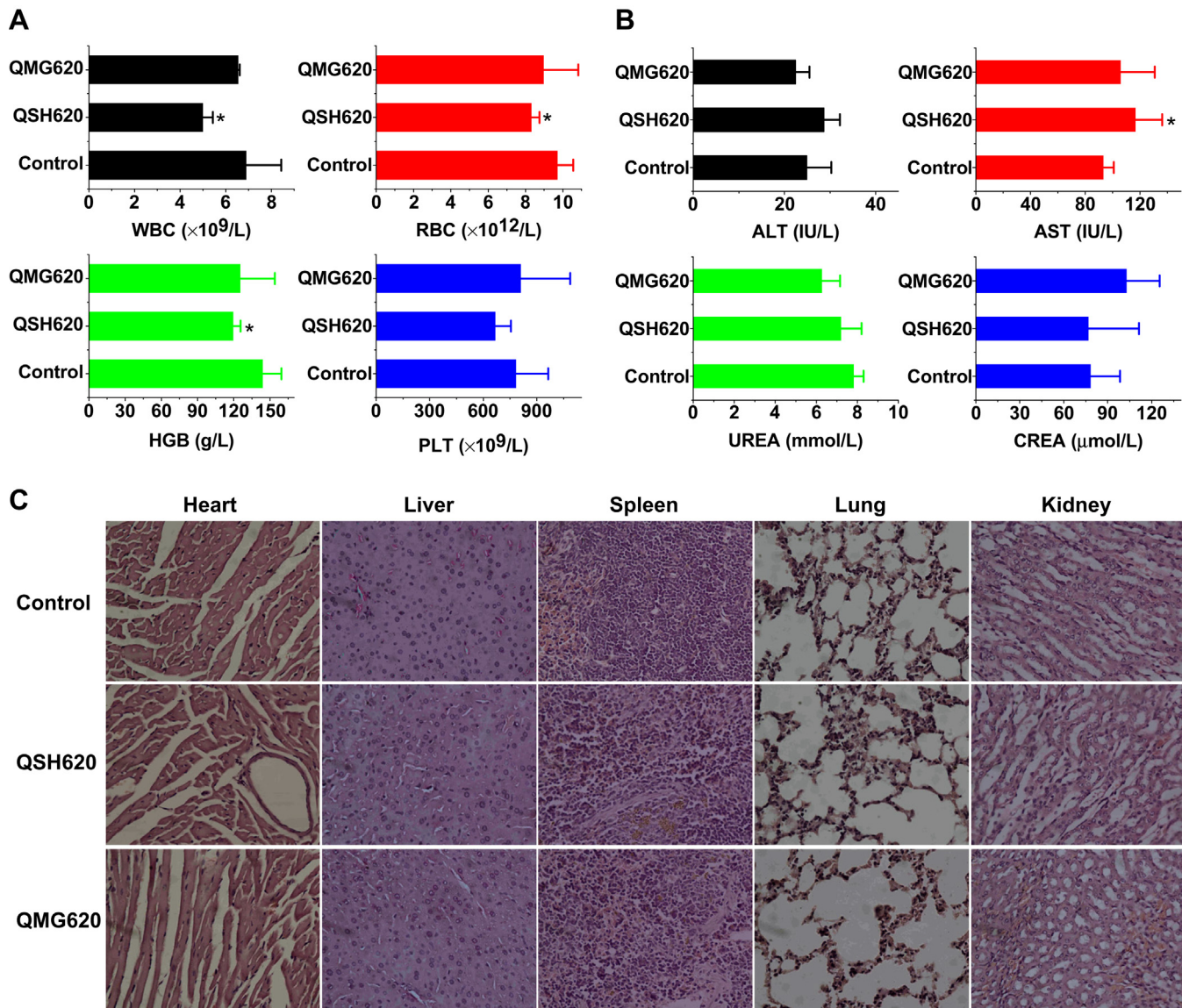


Fig. 8. Chronic toxicity evaluation of QSH620 and QMG620 15 weeks post-administration at 10 nmol/kg. A, Typical hematological parameters. B, Selected biomarkers related to liver/kidney functions. Results are expressed as mean \pm SD ($n = 6$). * $p < 0.05$ versus the control group. C, H&E stained sections of heart, liver, spleen, lung, and kidney which were resected from mice treated with QSH620 or QMG620 at 10 nmol/kg. The organs were harvested 15 weeks after administration. All images were taken at $\times 40$ magnification.

We then compared the toxicity of various QDs at a lower dose of 2.5 nmol/kg at a long-term of 15 w. Fifteen weeks post *i.v.* injection, the body weight of all QDs-treated mice was dramatically increased when compared with the corresponding weight at day 0 (Fig. S9B). In addition, QDs-administered mice did not show significant difference in the body weight versus the control group. Inspection on the organ index revealed no remarkable difference between various groups (Fig. 9A). The QSQ620 group displayed higher levels of ALT and AST when compared with the control group (Fig. 9B). Nevertheless, both ALT and AST concentrations were normal in the QSH620 and QMG620 groups. This suggested that a single administration of QSQ620 caused significant liver injury even after 15 w. This was further confirmed by examination on H&E sections (Fig. 9C). For the QSQ620 group, clear cellular edema could be observed in the liver. Moreover, the cytoplasm of some hepatocytes was loosened, resembling vacuole. Nevertheless, the morphology and integrity of hepatic lobules were well retained. In addition, the borderlines among portal triads were

clear. Reactive hyperplasia in the lymphoid follicles and hyperemia in the splenic sinus could be found for the QSQ620-treated mouse. Whereas similar toxicological profiles in the liver and spleen could be found for QSH620 and QMG620 groups, their degrees were slighter in comparison to the QSQ620 group. In the lung, hemorrhage, thickening of the pulmonary alveolar wall and reactive hyperplasia of lymph nodes were clearly present in the QSQ620 group. Furthermore, significant hyperplasia and swelling of glomerular capillary endothelium occurred in the kidney of the same group. Almost similar effects on the kidney were produced in the QSH620 and QMG620 groups.

In combination with acute toxicity study, above long-term examination suggested that chronic injuries were present for all the QDs-treated groups at both higher and lower doses, mainly due to the accumulation of QDs in specific organs such as the liver and spleen. In addition, injuries to kidney, the excretion organ, also existed for a long period of time. Among QDs with various coatings, the severest injury was found for the QSQ620 group.

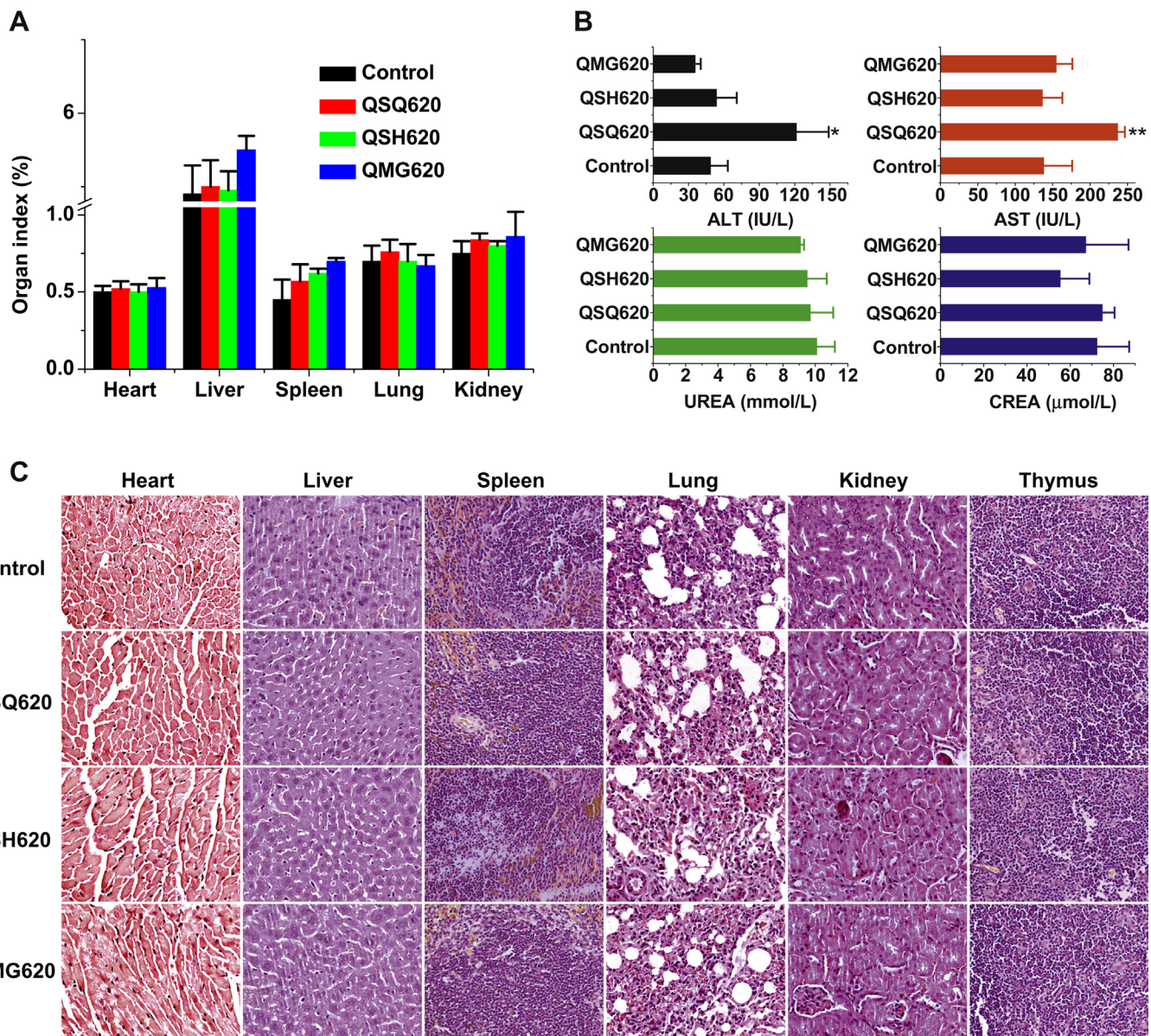


Fig. 9. Toxicity evaluation of various QDs 15 weeks after *i.v.* administration at 2.5 nmol/kg. A, The organ index. B, Typical biochemical markers of liver and kidney functions. * $p < 0.05$ versus the control group; ** $p < 0.01$ versus the control group. Data are mean \pm SD ($n = 6$). C, H&E stained pathophysiological sections of major organs from mice subjected to QDs treatment. All images were taken at $\times 40$ magnification.

3.5. Cationic polymer coating contributes to toxicity of positive QDs

It has been well documented that nanosystems based on cationic materials, such as cationic lipids and polycations like polyethylenimine (PEI) and poly(*L*-lysine) (PLL) may lead to cytotoxicity, hemolysis, thrombus formation, or tissue injury [63–65]. Accordingly, toxicity, especially the acute toxicity of positively charged QSQ620 should be mainly mediated by the coating polymer PDDA. Both *in vitro* and *in vivo* toxicity evaluation was then performed to confirm this hypothesis.

3.5.1. In vitro cytotoxicity

We compared the effect of various QDs and PDDA on the proliferation of ECV304 cells. As illustrated in Fig. S10A, no appreciable cell toxicity was observed for QSH620 and QMG620 at the examined doses varying from 0.0015625 to 0.1 nmol/mL. Significant cytotoxicity, however, could be found in the case of QSQ620. The calculated IC₅₀, the half maximal inhibitory concentration, for QSQ620 was 0.02 nmol/mL. Also, PDDA displayed dose-dependent toxicity (Fig. S10B), and its IC₅₀ against ECV304 was 0.02 mg/mL. Clearly, the disastrous cytotoxicity of QSQ620 was dominated by the positive coating of PDDA. It has been demonstrated that cationic polymers such as PEI and PLL may exert their cytotoxicity by causing necrotic-like damage or inducing cell apoptosis through mitochondria mediated pathways [65]. The positive moieties of these polymers are mainly responsible for the deleterious effects. As such, the quaternary ammonium group should largely account for the cytotoxicity of PDDA. According to thermogravimetric analysis, the corresponding PDDA concentration was 0.01 mg/mL at 0.02 nmol/mL of QSQ620. Consequently, *in vitro* cytotoxicity of QSQ620 was largely resulted from PDDA coating, while anchoring on QD nanocrystals amplified the cytotoxic effect of PDDA itself.

3.5.2. Acute toxicity

To further confirm the result derived from cell culture experiments, we compared *in vivo* acute toxicity of PDDA with that of QSQ620 in the BALB/c mouse model. After *i.v.* injection of various doses of PDDA or QSQ620, toxicity was evaluated by monitoring the appearance of shock, the survival and the mortality of animals, and the microscopic damage in the major tissues. Dose-dependent animal death could be observed for both PDDA and QSQ620 (Fig. 2B–D). In addition, the animal death generally occurred within 24 h, indicating acute phase toxicity. The calculated LD₅₀ of PDDA was 8.14 mg/kg. As indicated above, the LD₅₀ of QSQ620 was 7.16 nmol/kg, which corresponds to a PDDA dose of 4.53 mg/kg.

At either 8 or 10 nmol/kg, observation on H&E sections revealed swelling hepatocytes and vesicle-like cytoplasm in some hepatocytes of the liver collected immediately after animal death of QSQ620-treated mice (Fig. S11A). More serious injury in the liver was found at 6.4 nmol/kg of QSQ620, in which the edema of hepatocytes was more significant and extensive vesicular cytoplasm appeared. At lower doses of 4.096 and 5.12 nmol/kg, swelling hepatocytes with vesicular cytoplasm could also be observed, which are similar to those at 8 and 10 nmol/kg. This is reasonable in view of the fact that animal death may occur shortly after administration at high doses. At 10 nmol/kg, mice died about 1 h post injection, while animal death occurred within 3 h at 8 nmol/kg, mainly due to pulmonary embolism. In the case of PDDA, whereas high doses of PDDA (6.4, 8.0, and 10 mg/kg) resulted in hepatocellular swelling and vesicular cytoplasm, lower doses (4.096 and 5.12 mg/kg) did not cause discernable effect in the liver (Fig. S11B). In addition, we did not find significant abnormalities in the heart, spleen, lung, and kidney, when compared with the saline control.

Consequently, surface coating with cationic PDDA rendered positive QDs with more severe *in vitro* cytotoxicity and *in vivo* acute/

chronic toxicity, when compared with the negative and PEGylated QDs. Moreover, coating on QD nanocrystals may dramatically amplify the toxicity of PDDA polymer. Accordingly, it is paramount to choose biocompatible materials to decorate nanoparticles for biomedical applications, particularly when *in vivo* utilization is concerned.

4. Conclusions

In summary, QDs with various surface coatings displayed dramatically different biodistribution and *in vivo* toxicity. QDs coated with cationic polymer PDDA preferred to deposit in the lung rather than in the liver, while the negative and PEGylated QDs rendered abundant accumulation in the liver. With respect to acute phase toxicity, independent of surface coatings all QDs may elicit injuries in specific tissues to a certain degree. For positive QDs, their acute toxicity should be largely attributed to the coating material PDDA, while coating on nanoparticles may amplify *in vitro* and *in vivo* toxicity of PDDA. After a long period of 15 w, the chronic injuries were still present in all QD-treated mice. Nevertheless, PEGylated QDs showed the slightest injuries when compared with either positive or negative QDs. However, further comprehensive studies are still necessary to fully elucidate the interrelationships between biophysicochemical properties of nanoparticles and their *in vivo* biological effects, whereby establishing a powerful safety database to navigate clinic translation and shape subsequent regulation policies.

Acknowledgments

This study was financially supported by the National Natural Science Foundation of China (No. 81271695).

Appendix A. Supplementary data

Supplementary data related to this article can be found at <http://dx.doi.org/10.1016/j.biomaterials.2013.07.087>.

References

- [1] Kim BYS, Rutka JT, Chan WCW. Nanomedicine. *N Engl J Med* 2010;363:2434–43.
- [2] Torney F, Trewyn BG, Lin VSY, Wang K. Mesoporous silica nanoparticles deliver DNA and chemicals into plants. *Nat Nanotechnol* 2007;2:295–300.
- [3] Mortensen LJ, Oberdorster G, Pentland AP, DeLouise LA. In vivo skin penetration of quantum dot nanoparticles in the murine model: the effect of UVR. *Nano Lett* 2008;8:2779–87.
- [4] Bhabra G, Sood A, Fisher B, Cartwright L, Saunders M, Evans WH, et al. Nanoparticles can cause DNA damage across a cellular barrier. *Nat Nanotechnol* 2009;4:876–83.
- [5] Yamashita K, Yoshioka Y, Higashisaka K, Mimura K, Morishita Y, Nozaki M, et al. Silica and titanium dioxide nanoparticles cause pregnancy complications in mice. *Nat Nanotechnol* 2011;6:321–8.
- [6] Nel A, Xia T, Madler L, Li N. Toxic potential of materials at the nanolevel. *Science* 2006;311:622–7.
- [7] Kirchner C, Liedl T, Kudera S, Pellegrino T, Javier AM, Gaub HE, et al. Cytotoxicity of colloidal CdSe and CdSe/ZnS nanoparticles. *Nano Lett* 2005;5:331–8.
- [8] Jiang W, Kim BYS, Rutka JT, Chan WCW. Nanoparticle-mediated cellular response is size-dependent. *Nat Nanotechnol* 2008;3:145–50.
- [9] Verma A, Uzun O, Hu YH, Hu Y, Han HS, Watson N, et al. Surface-structure-regulated cell-membrane penetration by monolayer-protected nanoparticles. *Nat Mater* 2008;7:588–95.
- [10] Nel AE, Madler L, Velez D, Xia T, Hoek EMV, Somasundaran P, et al. Understanding biophysicochemical interactions at the nano-bio interface. *Nat Mater* 2009;8:543–57.
- [11] Cho EC, Au L, Zhang Q, Xia YN. The effects of size, shape, and surface functional group of gold nanostructures on their adsorption and internalization by cells. *Small* 2010;6:517–22.
- [12] Lewinski N, Colvin V, Drezek R. Cytotoxicity of nanoparticles. *Small* 2008;4:26–49.
- [13] Mahmoudi M, Azadmanesh K, Shokrgozar MA, Journeay WS, Laurent S. Effect of nanoparticles on the cell life cycle. *Chem Rev* 2011;111:3407–32.

- [14] Soenen SJ, Rivera-Gil P, Montenegro JM, Parak WJ, De Smedt SC, Braeckmans K. Cellular toxicity of inorganic nanoparticles: common aspects and guidelines for improved nanotoxicity evaluation. *Nano Today* 2011;6: 446–65.
- [15] Oberdorster G, Oberdorster E, Oberdorster J. Nanotoxicology: an emerging discipline evolving from studies of ultrafine particles. *Environ Health Perspect* 2005;113:823–39.
- [16] Dobrovolskaia MA, McNeil SE. Immunological properties of engineered nanomaterials. *Nat Nanotechnol* 2007;2:469–78.
- [17] Krug HF, Wick P. Nanotoxicology: an interdisciplinary challenge. *Angew Chem Int Ed* 2011;50:1260–78.
- [18] Alivisatos AP, Gu WW, Larabell C. Quantum dots as cellular probes. *Annu Rev Biomed Eng* 2005;7:55–76.
- [19] Smith AM, Duan HW, Mohs AM, Nie SM. Bioconjugated quantum dots for in vivo molecular and cellular imaging. *Adv Drug Deliv Rev* 2008;60:1226–40.
- [20] Zrazhevskiy P, Sena M, Gao XH. Designing multifunctional quantum dots for bioimaging, detection, and drug delivery. *Chem Soc Rev* 2010;39:4326–54.
- [21] Zhang LW, Monteiro-Riviere NA. Mechanisms of quantum dot nanoparticle cellular uptake. *Toxicol Sci* 2009;110:138–55.
- [22] Goso S, Gavello D, Giachello CNG, Franchino C, Carbone E, Carabelli V. The effect of CdSeZnS quantum dots on calcium currents and catecholamine secretion in mouse chromaffin cells. *Biomaterials* 2011;32:9040–50.
- [23] Chou LYT, Ming K, Chan WCW. Strategies for the intracellular delivery of nanoparticles. *Chem Soc Rev* 2011;40:233–45.
- [24] Chen N, He Y, Su YY, Li XM, Huang Q, Wang HF, et al. The cytotoxicity of cadmium-based quantum dots. *Biomaterials* 2012;33:1238–44.
- [25] Hoshino A, Fujioka K, Oku T, Suga M, Sasaki YF, Ohta T, et al. Physicochemical properties and cellular toxicity of nanocrystal quantum dots depend on their surface modification. *Nano Lett* 2004;4:2163–9.
- [26] Clift MJD, Varet J, Hankin SM, Brownlee B, Davidson AM, Brandenberger C, et al. Quantum dot cytotoxicity in vitro: an investigation into the cytotoxic effects of a series of different surface chemistries and their core/shell materials. *Nanotoxicology* 2011;5:664–74.
- [27] Walkey CD, Olsen JB, Guo HB, Emili A, Chan WCW. Nanoparticle size and surface chemistry determine serum protein adsorption and macrophage uptake. *J Am Chem Soc* 2011;134:2139–47.
- [28] Derfus AM, Chan WCW, Bhatia SN. Probing the cytotoxicity of semiconductor quantum dots. *Nano Lett* 2004;4:11–8.
- [29] Hardman R. A toxicologic review of quantum dots: toxicity depends on physicochemical and environmental factors. *Environ Health Perspect* 2006;114:165–72.
- [30] Lee J, Lilly GD, Doty RC, Podsiadlo P, Kotov NA. In vitro toxicity testing of nanoparticles in 3D cell culture. *Small* 2009;5:1213–21.
- [31] Lin PP, Chen JW, Chang LW, Wu JP, Redding L, Chang H, et al. Computational and ultrastructural toxicology of a nanoparticle, quantum dot 705, in mice. *Environ Sci Technol* 2008;42:6264–70.
- [32] Hauck TS, Anderson RE, Fischer HC, Newbigging S, Chan WCW. In vivo quantum-dot toxicity assessment. *Small* 2010;6:138–44.
- [33] Lin CH, Yang MH, Chang LW, Yang CS, Chang H, Chang WH, et al. Cd/Se/Te-based quantum dot 705 modulated redox homeostasis with hepatotoxicity in mice. *Nanotoxicology* 2011;5:650–63.
- [34] Liu W, Zhang SP, Wang LX, Qu C, Zhang CW, Hong L, et al. CdSe quantum dot (QD)-induced morphological and functional impairments to liver in mice. *PLoS ONE* 2011;6:e24406.
- [35] Ho CC, Chang H, Tsai HT, Tsai MH, Yang CS, Ling YC, et al. Quantum Dot 705, a cadmium-based nanoparticle, induces persistent inflammation and granuloma formation in the mouse lung. *Nanotoxicology* 2013;7:105–15.
- [36] Ye L, Yong KT, Liu LW, Roy I, Hu R, Zhu J, et al. A pilot study in non-human primates shows no adverse response to intravenous injection of quantum dots. *Nat Nanotechnol* 2012;7:453–8.
- [37] Ambrosone A, Mattera L, Marchesano V, Quarta A, Susha AS, Tino A, et al. Mechanisms underlying toxicity induced by CdTe quantum dots determined in an invertebrate model organism. *Biomaterials* 2012;33:1991–2000.
- [38] Roberts JR, Antonini JM, Porter DW, Chapman RS, Scabilloni JF, Young SH, et al. Lung toxicity and biodistribution of Cd/Se-ZnS quantum dots with different surface functional groups after pulmonary exposure in rats. *Part Fibre Toxicol* 2013;10:1–17.
- [39] Fischer HC, Liu LC, Pang KS, Chan WCW. Pharmacokinetics of nanoscale quantum dots: in vivo distribution, sequestration, and clearance in the rat. *Adv Funct Mater* 2006;16:1299–305.
- [40] Yang RSH, Chang LW, Wu JP, Tsai MH, Wang HJ, Kuo YC, et al. Persistent tissue kinetics and redistribution of nanoparticles, quantum dot 705, in mice: ICP-MS quantitative assessment. *Environ Health Perspect* 2007;115:1339–43.
- [41] Choi HS, Liu WH, Misra P, Tanaka E, Zimmer JP, Ipe BI, et al. Renal clearance of quantum dots. *Nat Biotechnol* 2007;25:1165–70.
- [42] Fitzpatrick JAJ, Andreko SK, Ernst LA, Waggoner AS, Ballou B, Bruchez MP. Long-term persistence and spectral blue shifting of quantum dots in vivo. *Nano Lett* 2009;9:2736–41.
- [43] Schipper ML, Lyer G, Koh AL, Cheng Z, Ebenstein Y, Aharoni A, et al. Particle size, surface coating, and PEGylation influence the biodistribution of quantum dots in living mice. *Small* 2009;5:126–34.
- [44] Gil PR, Oberdorster G, Elder A, Puntes V, Parak WJ. Correlating physico-chemical with toxicological properties of nanoparticles: the present and the future. *ACS Nano* 2010;4:5527–31.
- [45] Li JJ, Wang YA, Guo WZ, Keay JC, Mishima TD, Johnson MB, et al. Large-scale synthesis of nearly monodisperse CdSe/CdS core/shell nanocrystals using air-stable reagents via successive ion layer adsorption and reaction. *J Am Chem Soc* 2003;125:12567–75.
- [46] Sun QJ, Wang YA, Li LS, Wang DY, Zhu T, Xu J, et al. Bright, multicoloured light-emitting diodes based on quantum dots. *Nat Photonics* 2007;1:717–22.
- [47] Gao XH, Cui YY, Levenson RM, Chung LWK, Nie SM. In vivo cancer targeting and imaging with semiconductor quantum dots. *Nat Biotechnol* 2004;22: 969–76.
- [48] Geys J, Nemmar A, Verbeken E, Smolders E, Ratoi M, Hoylaerts MF, et al. Acute toxicity and prothrombotic effects of quantum dots: impact of surface charge. *Environ Health Perspect* 2008;116:1607–13.
- [49] Yu WW, Qu LH, Guo WZ, Peng XG. Experimental determination of the extinction coefficient of CdTe, CdSe, and CdS nanocrystals. *Chem Mater* 2003;15:2854–60.
- [50] Choi HS, Liu WH, Liu FB, Nasr K, Misra P, Bawendi MG, et al. Design considerations for tumour-targeted nanoparticles. *Nat Nanotechnol* 2010;5:42–7.
- [51] Kim S, Lim YT, Solesz EG, De Grand AM, Lee J, Nakayama A, et al. Near-infrared fluorescent type II quantum dots for sentinel lymph node mapping. *Nat Biotechnol* 2004;22:93–7.
- [52] So MK, Xu CJ, Loening AM, Gambhir SS, Rao JH. Self-illuminating quantum dot conjugates for in vivo imaging. *Nat Biotechnol* 2006;24:339–43.
- [53] Yong KT, Roy I, Ding H, Bergey EJ, Prasad PN. Biocompatible nar-infrared quantum dots as ultrasensitive probes for long-term in vivo imaging applications. *Small* 2009;5:1997–2004.
- [54] Chang E, Thekkedath N, Yu WW, Colvin VL, Drezek R. Evaluation of quantum dot cytotoxicity based on intracellular uptake. *Small* 2006;2:1412–7.
- [55] Hauck TS, Ghazani AA, Chan WCW. Assessing the effect of surface chemistry on gold nanorod uptake, toxicity, and gene expression in mammalian cells. *Small* 2008;4:153–9.
- [56] Fischer D, Dautzenberg H, Kunath K, Kissel T. Poly(diallyldimethylammonium chlorides) and their N-methyl-N-vinylacetamide copolymer-based DNA-polymers: role of molecular weight and charge density in complex formation, stability, and in vitro activity. *Int J Pharm* 2004;280:253–69.
- [57] Krajcik R, Jung A, Hirsch A, Neuhuber W, Zolk O. Functionalization of carbon nanotubes enables non-covalent binding and intracellular delivery of small interfering RNA for efficient knock-down of genes. *Biochem Biophys Res Commun* 2008;369:595–602.
- [58] Meli LD, Mamizuka EM, Carmona-Ribeiro AM. Antimicrobial particles from cationic lipid and polyelectrolytes. *Langmuir* 2010;26:12300–6.
- [59] Bertrand N, Leroux JC. The journey of a drug-carrier in the body: an anatomico-physiological perspective. *J Control Release* 2012;161:152–63.
- [60] Kutscher HL, Chao P, Deshmukh M, Singh Y, Hu P, Joseph LB, et al. Threshold size for optimal passive pulmonary targeting and retention of rigid nanoparticles in rats. *J Control Release* 2010;143:31–7.
- [61] Moghimi SM, Hunter AC, Murray JC. Long-circulating and target-specific nanoparticles: theory to practice. *Pharmacol Rev* 2001;53:283–318.
- [62] Harrison KL. Fetal erythrocyte lifespan. *Aust Paediatr J* 1979;15:96–7.
- [63] Chollet P, Favrot MC, Hurbin A, Coll JL. Side-effects of a systemic injection of linear polyethylenimine-DNA complexes. *J Gene Med* 2002;4:84–91.
- [64] Akagi D, Oba M, Koyama H, Nishiyama N, Fukushima S, Miyata T, et al. Biocompatible micellar nanovectors achieve efficient gene transfer to vascular lesions without cytotoxicity and thrombus formation. *Gene Ther* 2007;14: 1029–38.
- [65] Hunter AC, Moghimi SM. Cationic carriers of genetic material and cell death: a mitochondrial tale. *Biochim Biophys Acta* 2010;1797:1203–9.